Nano Research 2013, 6(7): 571–580
DOI 10.1007/s12274-013-0332-8
Research Article
ISSN 1998-0124
CN 11-5974/O4

Hybrid PdAg alloy–Au nanorods: Controlled growth, optical properties and electrochemical catalysis

Qiao Zhang[1,2], Xia Guo[1], Zhenxing Liang[1,2], Jianhuang Zeng[1,2], Jian Yang[1,3] (✉), and Shijun Liao[1,2] (✉)

[1] *School of Chemistry and Chemical Engineering, South China University of Technology, Guangzhou 510640, China*
[2] *Key Laboratory of Fuel Cell Technology of Guangdong Province, Guangzhou 510640, China*
[3] *Department of Chemistry, Shandong University, Jinan 250100, China*

Received: 28 February 2013
Revised: 10 May 2013
Accepted: 12 May 2013

KEYWORDS
nanostructures,
hybrid materials,
metals,
controlled growth,
electrochemical catalysis,
optical properties

ABSTRACT

Controllable growth of high-quality hybrid nanostructures is highly desirable for the fabrication of hierarchical, complex and multifunctional devices. Here, PdAg alloys have been controllably grown at different locations on gold nanorods, producing dumbbell-like nanostructures with PdAg at the ends of the gold nanorods or branched nanostructures with PdAg grown almost perpendicular to the gold nanorods. The nucleation sites of PdAg alloys on the gold nanorods can be effectively tuned by varying the concentrations of H_2PdCl_4, $AgNO_3$ and cetyltrimethylammonium bromide (CTAB). The dumbbell-like and branched nanostructures were characterized by transmission electron microscopy (TEM), high-resolution TEM (HRTEM), line-scanning energy-dispersive X-ray spectroscopy (EDS), X-ray photoelectron spectroscopy (XPS) and UV–Vis absorption spectroscopy. Their electrocatalytic performance was evaluated using ethanol oxidation as a probe reaction. The dumbbell-like nanostructures show a better anti-poisoning performance, but a worse electrochemical activity than the branched ones. The results provide guidelines for the controlled growth of complicated nanostructures for either fundamental studies or potential applications.

1 Introduction

High-quality hybrid nanocomposites with well-defined building blocks, narrow size distributions and tailorable physical properties, are highly desirable for a myriad of applications, such as ultrasensitive detection, lithium ion batteries, and heterogeneous catalysis [1–4]. Since the performance of nanocomposites in these fields strongly depends on the shape and size of their component building blocks, how to control their growth has become very important, posing great challenges in synthesis [5]. In the case of one-dimensional metallic nanocomposites, controlled growth can generate two distinctive architectures: Dumbbell-like nanorods composed of different materials in a linear arrangement, and branched nanorods consisting of different materials

Address correspondence to Jian Yang, yangjian@scut.edu.cn; Shijun Liao, chsjliao@scut.edu.cn

in a perpendicular orientation. Both of these have been attracting intense interest [6–12]. However, the difficulties in synthesis greatly limit the further exploration of their physical properties and potential applications. For example, Chaudret et al. fabricated dumbbell-like Au-tipped Co nanorods through a galvanic replacement between [AuCl(PPh)$_3$] and Co nanorods [6]. But the application of this method to other dumbbell-like nanorods is limited by the usage of expensive and toxic organometallic compounds. Song et al. synthesized Ag-tipped Au nanorods at an elevated temperature, using multiply twinned gold nanorods as a seed [7]. As a result of the high temperatures employed, the size of the dumbbell-like nanorods was always on the order of hundreds of nanometers, which has an adverse effect on the optical properties and subsequent biological applications. In order to address this issue, a low-temperature approach was developed for the fabrication of dumbbell-like Ag-tipped Au nanorods with a mixture of binary surfactants [8]. However all the studies reported to date involve the preferential growth of a single metal at sites on another metallic nanorod.

Compared with dumbbell-like bimetallic nanorods, branched nanorods have been studied to a lesser extent [13–15]. Xia et al. reported the use of truncated octahedral Pd nanocrystals as a seed to prepare Pd-supported Pt branches [1]. The as-obtained Pd–Pt nanodendrites exhibited an excellent electrocatalytic activity for the oxygen reduction reaction. A similar strategy was also employed for the synthesis of Au–Pt bimetallic nanostructures in a mixture of diphenyl ether and oleylamine [13]. Recently, gold nanorods coated with PdPt alloy nanodots have also been reported [14]. The Au@PdPt nanorods presented fair catalytic activities in several reactions, such as the oxidation of ascorbic acid, and the reduction of *p*-nitrophenol.

Here, a simple and convenient method is developed to achieve the preferential growth of PdAg alloys along, or perpendicular to, Au nanorods, producing high-quality dumbbell-like or branched nanocomposites. The growth process is conducted at nearly room temperature without the usage of toxic organometallics, multiple-twinned seeds, or expensive surfactants. At the same time, it successfully realizes the simultaneous control over the formation of metallic alloys and their nucleation/growth sites. The introduction of preferential growth of alloys also offers a number of opportunities to utilize the unique properties of alloys, which have been widely documented in many previous applications [16–18]. To the best of our knowledge, dumbbell-like nanorods based on alloy tips have not been reported before. The controlled growth of PdAg alloys on the gold nanorods also provides an effective way to manipulate their optical properties. Finally, the electrocatalytic activities of these PdAg–Au nanorods are explored using ethanol oxidation as a probe reaction.

2 Experimental

2.1 Chemicals and instruments

$HAuCl_4 \cdot xH_2O$ (x = 3–5, Au ~47.8%), and cetyltrimethylammonium bromide (CTAB, ≥ 99%) were obtained from July Chemical Co. Ltd and Bio-Life Sci. & Tech. Co. Ltd in Shanghai. $PdCl_2$ (Pd ≥ 59.0%), $AgNO_3$ (≥ 99.8%) and $NaBH_4$ (≥ 96%) were purchased from Sinopharm Chemical Reagent Co. Ltd also in Shanghai. Ascorbic acid (≥ 99.7%) was obtained from Guanghua Chemical Factory Co. Ltd in Guangzhou. A commercial Pd/C (10% Pd) catalyst was obtained from Sigma Aldrich (No. 205699). All the reagents were used without any further purification.

Low-magnification transmission electron microscopy (TEM) images were acquired with a transmission electron microscope (FEI Tecnai 12) at an accelerating voltage of 100 kV. High-resolution TEM (HRTEM) images and energy-dispersive X-ray spectra (EDS) were acquired on an analytical transmission electron microscope (JEOL 2010 at 200 kV). The samples for TEM imaging were purified by centrifugation before the observation, in order to remove the surfactants or excess reactants. Then, the samples were dispersed in distilled water. The resulting solution was dropped on a copper grid coated with an amorphous carbon film. X-ray photoelectron spectra (XPS) were recorded with an AXIS Ultra DLD spectrometer (Kratos Anal.), using the Al Kα line as the excitation source. The calibration was conducted by referring the C1s signal of the contaminating carbon to the binding energy of 284.6 eV. UV–Vis absorption spectra were recorded in

the range 300–900 nm with a Shimadzu 2450 spectrophotometer at room temperature.

2.2 Controllable growth of PdAg alloys on Au nanorods

High-quality gold nanorods were prepared via a typical seed-mediated growth process [19, 20]. The gold nanorods were purified by centrifugation twice at 10,000 rpm for 10 min and then dispersed in distilled water. In a typical procedure for dumbbell-like nanorods, 0.6 mL of 100 mM CTAB, 50 μL of 2 mM H_2PdCl_4, 45 μL of 4 mM $AgNO_3$, and 2 mL of purified gold nanorods were mixed together and heated to 40 °C for 30 min. After that, a large excess of ascorbic acid was introduced into the solution. The volume of the solution was kept at 6 mL by adding distilled water. After 3 h at 40 °C, the gray solution was cooled down to room temperature. The product was collected by centrifugation and dispersed in distilled water for later characterization. The branched nanorods were produced in increasing yield, as the volume of H_2PdCl_4 was increased to 300 μL.

2.3 Electrochemical catalysis of ethanol oxidation

The electrocatalytic performances of the PdAg alloy–gold nanorods with different architectures were evaluated in a three-electrode cell with a glassy carbon rotating disk electrode as the working electrode, a platinum wire as the counter electrode, and Hg/HgO (1 M KOH) as the reference electrode. The data were collected by an electrochemical station (Ivium, Netherlands). For electrochemical measurements, 10 μL of the nanorods with different architectures was added to 100 μL of 0.05 wt.% Nafion solution. After sonicating for 10 min, 10 μL of the solution was dropped onto the working electrode for cyclic voltammetry (CV). The blank CV was carried out in 1.0 M KOH in the potential range 0.25 to –0.92 V at a scan rate of 50 $mV \cdot s^{-1}$ at room temperature. Then, the electrochemically active surface areas (ECSA) were calculated and normalized based on the reduction of PdO_x. After that, CVs were conducted in 1.0 M KOH/1.0 M ethanol with the same potential range and scan rate. All the electrolytes were purged with nitrogen for 30 min before each measurement.

3 Results and discussion

The dumbbell-like PdAg-tipped gold nanorods were prepared by reducing a mixture of H_2PdCl_4 and $AgNO_3$ with the gold nanorods as a seed under mild experimental conditions. Figure 1(a) shows a TEM image of the product after the reaction. The product displays a typical rod-like shape and a narrow size distribution, both of which might be inherited from the gold nanorods. A high-magnification TEM image of the nanorods (Fig. 1(b)) reveals the dumbbell-like feature, which has not previously been observed for gold nanorods (Fig. S1 in the Electronic Supplementary Material (ESM)). Furthermore, there is a contrast difference at the tips of the dumbbell-like nanorods, which is likely to be caused by the deposition of Pd and Ag. This speculation is in good agreement with the results obtained by elemental analysis of the dumbbell-like nanorods (Fig. S2 in the ESM). The elemental analysis data along the axial direction of the dumbbell-like nanorod (Fig. 1(d)) show that Pd and Ag are highly concentrated, indicative of preferential growth of Pd and Ag at the tips of the gold nanorods. Because the signal intensities of both Pd and Ag reach a maximum simultaneously, this suggests that Pd and Ag form an alloy, which is also supported by HRTEM images (Fig. 1(c)) and XPS spectra (Fig. 2).

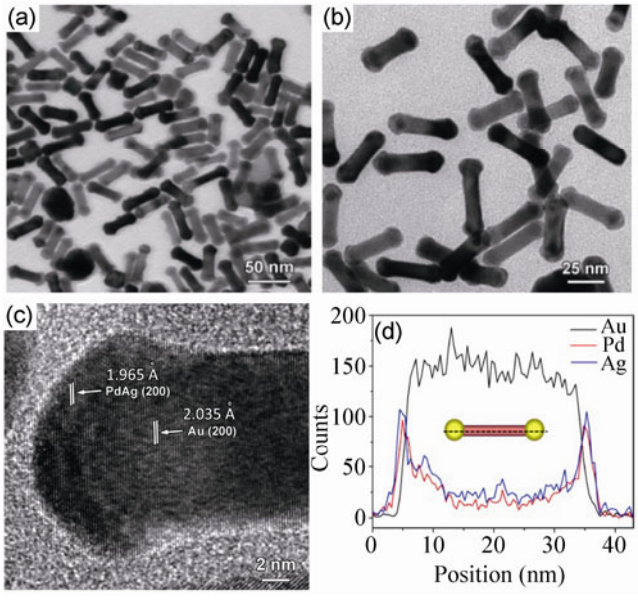

Figure 1 (a) and (b) TEM images, (c) HRTEM image, and (d) line-scanning EDS spectrum of the dumbbell-like PdAg–Au nanorods.

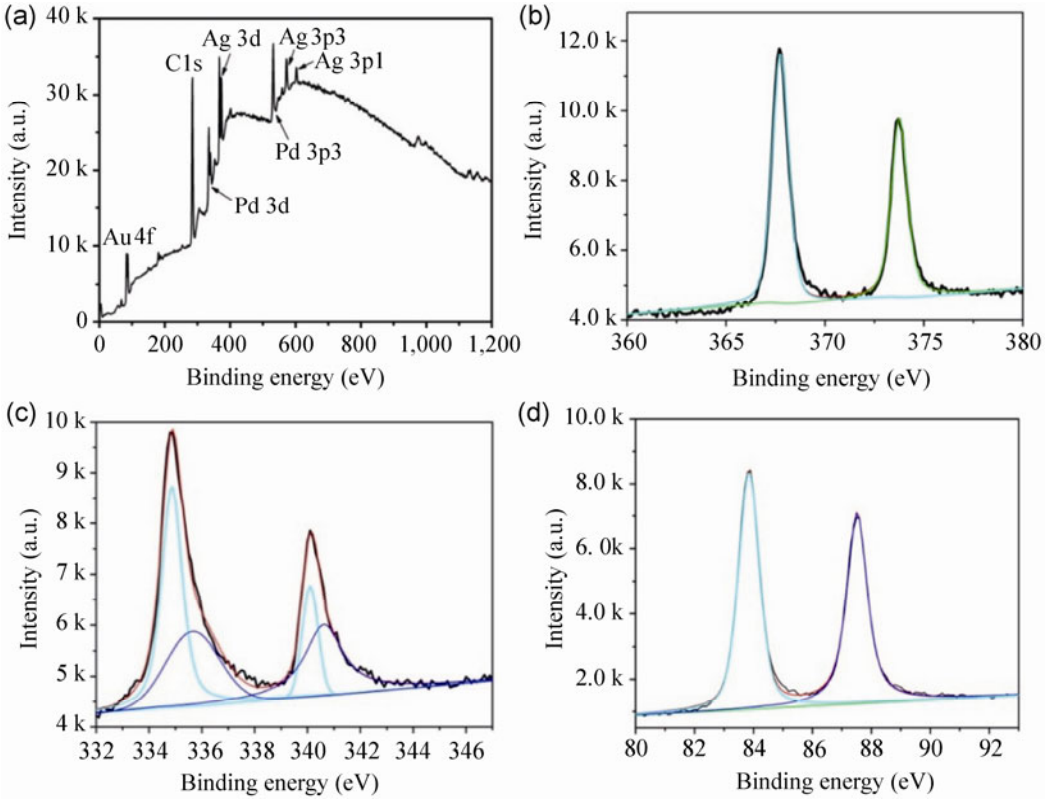

Figure 2 XPS spectra of the PdAg–Au dumbbell-like nanorods. (a) Survey spectrum, (b)–(d) the high resolution spectra of Ag 3d, Pd 3d, Au 4f.

As shown in Fig. 1(c), the dumbbell-like nanorod exhibits a typical single-crystal nature, indicating the epitaxial growth of PdAg at the tips of the gold nanorods. The lattice distances between neighboring fringes at the tip and body of the dumbbell-like nanorod are 1.965 and 2.035 Å respectively, corresponding to the crystal planes of PdAg (200) and Au (200). It is believed that since Pd, Ag and Au have the same crystal structure and small lattice mismatches (4.6% for Pd/Au, 0.2% for Ag/Au and 4.8% for Pd/Ag), this facilitates the epitaxial growth of PdAg on gold nanorods and help to retain the single-crystal nature of the nanorods. Compared to Pd, Ag exhibits a lower lattice mismatch and a better affinity to Au. However, Ag ions have a lower electrochemical potential than Pd ions [21], slowing down the formation of Ag. The combination of these two effects makes Pd and Ag ions synchronously reduced on the surface of the gold nanorods. This result is also confirmed by control experiments with Pd^{2+} ions or Ag^{+} ions individually (Fig. S3 in the ESM): Both of these ions could be separately reduced at this temperature.

The preferential growth of PdAg at the tips of the gold nanorods might be related to the slow reaction rate caused by the low concentration of the reactants in solution. The slow reaction rate makes the nucleation events favor surface sites with high chemical potentials; these are usually high-index crystal facets, are less surface-passivated, and/or have large surface curvature. In the case of the gold nanorods, most of these surface sites are located at the tips. So, PdAg will preferentially nucleate and grow at the tips of the gold nanorods. Similar growth has been documented for a few other examples, such as Ag–Au–Ag, Au–Co–Au, and Pt–Au–Pt nanodumbbells [7–12]. In contrast to previous reports [6–12], the ends of the nanodumbbells in our case are covered by bimetallic species, which is generally more difficult to achieve due to the requirement to incorporate more elements in the preferential growth.

Figure 2 shows the XPS spectra of the dumbbell-like PdAg–Au nanorods. The survey spectrum (Fig. 2(a)) clearly shows the presence of Ag, Pd and Au in the product. More details about the chemical status of these elements could be achieved from their high-resolution spectra. As presented in Fig. 2(b), there are two strong signals at 367.7 and 373.3 eV, which could be attributed to the $3d_{5/2}$ and $3d_{3/2}$ binding energies of elemental silver [22–24]. In contrast to the spectrum for Ag 3d, the high-resolution spectrum of Pd 3d shows two asymmetric signals (Fig. 2(c)), indicating there are multiple palladium species on the surface. Based on a Gaussian model, there are two palladium species on the surface of the dumbbell-like nanorods. The dominant doublet at 334.4 and 339.6 eV corresponds to $3d_{5/2}$ and $3d_{3/2}$ signals of elemental palladium [22–24]. The weaker doublet at 335.2 and 340.2 eV can be associated with oxidized palladium species on the surface that probably arise from the surface oxidization due to the exposure to air. The molar ratio of Pd/Ag is 0.65, very close to that from EDS spectra (0.69). This result also excludes the possibility of a core–shell structure of Pd and Ag, but agrees well with the proposed alloy nature of PdAg. Figure 2(d) shows the signals of Au 4f at 83.4 and 87.1 eV, consistent with the reported data for elemental gold [22].

The ratio of Pd/Ag at the ends of the dumbbell-like nanorods could be tuned by using different amounts of $AgNO_3$. As shown in Figs. 3(a)–3(c), all the products retained the dumbbell-like shape when the volume of $AgNO_3$ solution was varied from 15 μL to 90 μL. This indicates that there is a broad concentration window of $AgNO_3$ available for the formation of the dumbbell-like nanorods, which makes this experiment highly reproducible. EDS spectra give Pd/Ag molar ratios of 1.29 for 15 μL of $AgNO_3$ solution and 0.55 for 90 μL, consistent with the change of $H_2PdCl_4/AgNO_3$ ratio in the solution. This provides an effective way to tune the composition of the alloy at the ends of the dumbbell-like nanorods.

The optical properties of metal nanoparticles, particularly for Ag and Au, are very sensitive to their composition, size and shape. For example, when the gold nanorods are coated by a silver layer, both transverse surface plasmon resonance (TSPR) and longitudinal surface plasmon resonance (LSPR) absorptions are

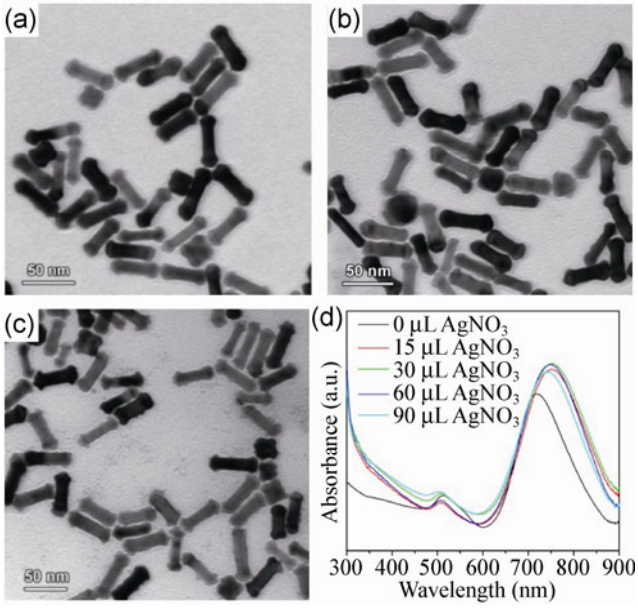

Figure 3 (a)–(c) TEM images and (d) UV–Vis absorption spectra of dumbbell-like PdAg–Au nanorods obtained with different amounts of 4 mM $AgNO_3$: (a) 15 μL, (b) 60 μL, (c) 90 μL. Other conditions: 2 mM H_2PdCl_4, 50 μL; CTAB, 0.01 M; Temp., 40 °C.

greatly shifted to the blue [25]. However, if Ag only grows at the tips of the Au nanorods, the LSPR absorption exhibits a slight red-shift [8, 12], which is similar to our case. Figure 3(d) shows the absorption spectra of the dumbbell-like nanorods. Basically, they preserve the absorption features of the gold nanorods. But the TSPR absorption slightly shifts to the blue in comparison with that of the original gold nanorods and the LSPR absorption moves to the longer wavelength. The opposite shifts of the TSPR and LSPR absorptions probably comes from the increase in the aspect ratio of the nanorods, which is consistent with the results reported for dumbbell-like nanorods in the Ref. [12, 26].

The influence of the amount of H_2PdCl_4 on the product is totally different from the case of $AgNO_3$. The dumbbell-like nanorods are the dominant product (Fig. 4(a)), when the volume of H_2PdCl_4 was 0.05 mL. As the volume of H_2PdCl_4 solution was increased to 0.10 and 0.20 mL, the PdAg alloy starts to grow on the body of the gold nanorods, producing a quite rough surface (Figs. 4(b) and 4(c)). This result implies that the preferential growth of PdAg at the ends of the gold nanorods is weakened. This phenomenon becomes more significant for 0.30 mL of H_2PdCl_4. In this case, the gold nanorods are completely coated by a large

number of tiny rods on the surface of the gold nanorods, as shown in Fig. 4(d). The tiny rods are nearly perpendicular to the surface, and have a diameter of 3–5 nm and length of 6–10 nm. HRTEM images (Figs. 4(e) and 4(f)) confirm the epitaxial growth of the tiny rods on the gold nanorods. The formation of the tiny rods can be explained by the fast nucleation and growth rate of the alloy, which has been documented for a number of one-dimensional structures [27, 28]. For example, Kang et al. lowered the potential of a working electrode to increase the supersaturation of the product and the crystal growth rate, producing dendritic CuNi alloy [27]. Such a branched structure has been seldom reported for gold nanorods, although surface coating of gold nanorods with small nanoparticles has been reported in a few cases [14, 29, 30].

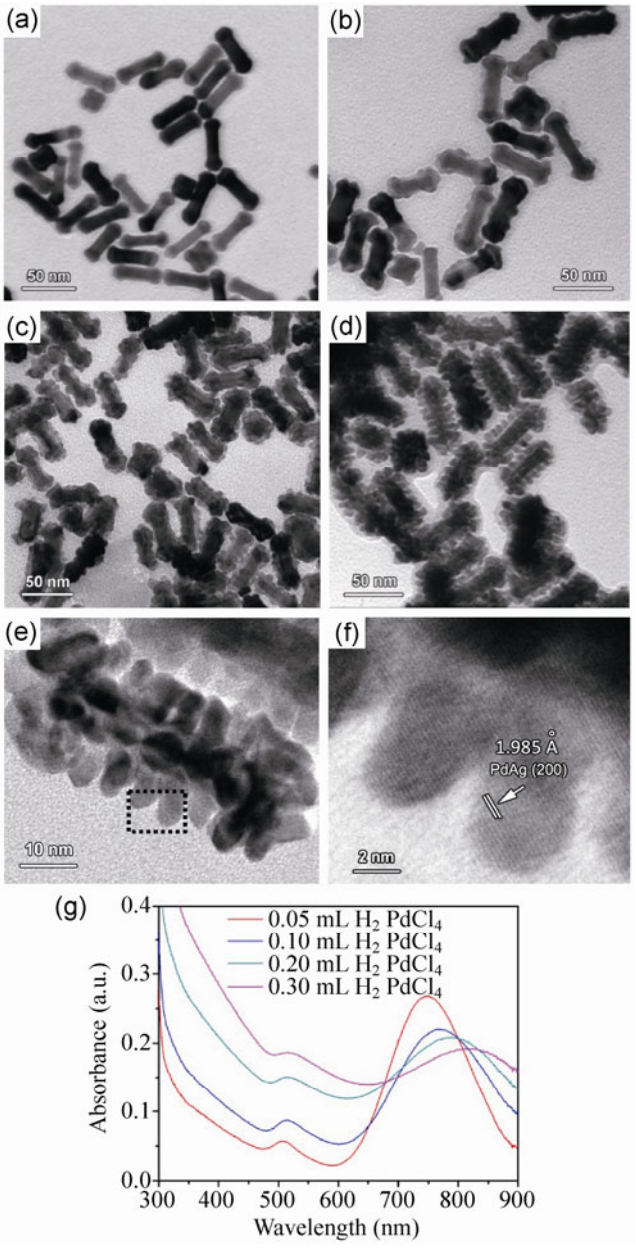

Figure 4 TEM images of the product obtained with different amounts of 2 mM H_2PdCl_4: (a) 0.05 mL, (b) 0.10 mL, (c) 0.20 mL, (d) 0.30 mL. (e) and (f) HRTEM images of the branched nanorods in (d). (g) UV–Vis absorption spectra of these products. Other conditions: 4 mM $AgNO_3$, 60 μL; CTAB, 0.01 M; Temp., 40 ˚C.

Both the TSPR and LSPR absorptions of the branched nanorods gradually moved to longer wavelengths (Fig. 4(g)), as the amount of H_2PdCl_4 was increased. Such a red-shift could be associated with the formation of the rough surface along the nanorods caused by the growth of PdAg. A similar result was also observed in the case of deposition of small nanoparticles on gold nanorods [14, 29]. In addition, the TSPR and LSPR absorptions quickly broaden in our case, which might result from the SPR damping and the broad size distribution of the nanorods due to the presence of alloys.

The control over the growth from the branched nanorods to the dumbbell-like ones, could be also achieved by varying the concentration of CTAB. Figure 5 shows TEM images of the products obtained with different concentrations of CTAB with the amounts of $AgNO_3$ and H_2PdCl_4 fixed at 30 μL of 4 mM solution and 300 μL of 2 mM solution, respectively. When the concentration of CTAB in the reaction was 10 mM, branched nanorods could be easily visualized in the product, as shown in Fig. 5(a). After the concentration of CTAB was increased to 40 mM, the product was dominant by nanorods with two bulky ends (Fig. 5(b)), rather than branched nanorods. A higher concentration of CTAB of 200 mM makes this feature even more significant, as shown in Fig. 5(c). The results clearly indicate that a high concentration of CTAB favors the preferential growth at the ends of the gold nanorods [19, 20]. Meanwhile, the size of the alloy component of the dumbbell-like nanorods in Fig. 5(c) is much larger than those in Fig. 3, indicating a possible way to tailor the size of the alloy component at the ends of the gold nanorods.

Since Pd, Au and Ag are noble metals, the electrocatalytic activity of the hybrid nanorods was evaluated

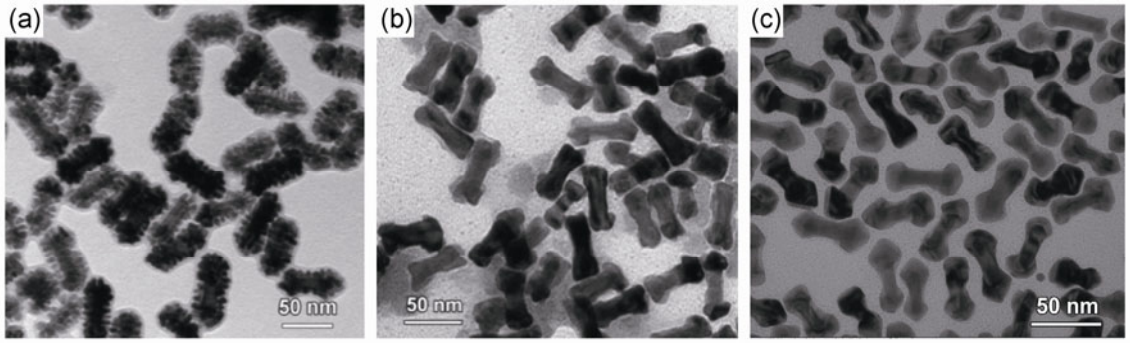

Figure 5 TEM images of the product obtained at different concentrations of CTAB: (a) 10 mM, (b) 40 mM, (c) 200 mM. Other conditions: 4 mM $AgNO_3$, 30 μL; 2 mM H_2PdCl_4, 300 μL; Temp., 40 ˚C.

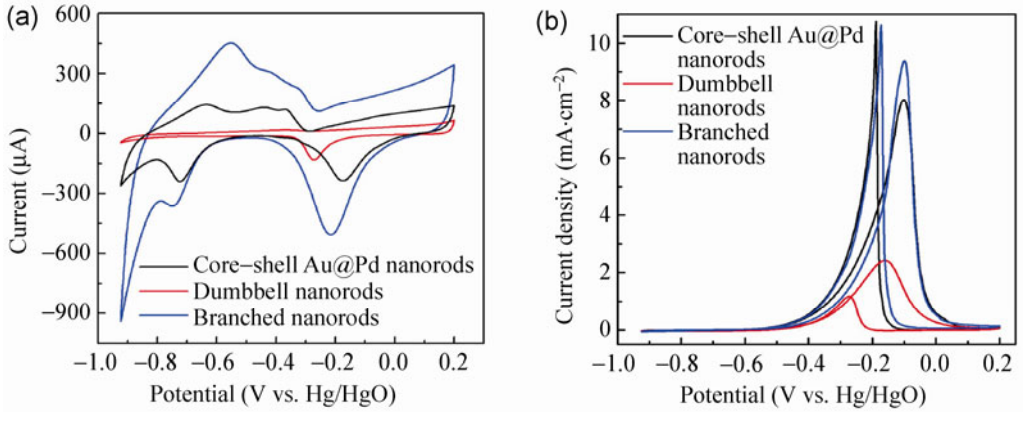

Figure 6 Cyclic voltammetric measurements for the different nanorods in (a) 1.0 M KOH, and (b) 1.0 M KOH + 1.0 M ethanol.

using the ethanol oxidation reaction (EOR) in alkaline electrolyte as a probe reaction. Figure 6(a) shows the CV profiles of core–shell Au@Pd nanorods, dumbbell-like and branched hybrid nanorods in 1.0 M KOH without ethanol. Here, the core–shell Au@Pd nanorods were prepared based on the reported protocols [31]. All three nanorods exhibit similar columbic features in the CV profiles, such as the formation and reduction of PdO_x, and the adsorption and desorption of H_2 [32, 33]. Compared with the reduction of PdO_x in the core–shell Au@Pd nanorods, the reduction processes for the branched and dumbbell-like nanorods shift to negative positions, indicating that the electronic structure of the nanorods has been changed after alloying with Ag. Moreover, the shift increases with the content of Ag in the PdAg alloy. For the gold nanorods and the core–shell Au@Ag nanorods [25], no redox chemistry occurs during the scans (Fig. S4 in the ESM), suggesting Pd is the electroactive component. The ECSA of the catalysts were extracted by the coulometric charge correlated with the reduction of PdO_x and then compared with a commercial Pd/C catalyst, as summarized in Table S1 (in the ESM).

The electrocatalytic activities of the branched nanorods, the dumbbell-like nanorods, and the core–shell Au@Pd nanorods for the EOR are illustrated by the CV profiles in Fig. 6(b). The voltammetric features of the CV profiles are in agreement with the reported electrooxidation of ethanol in alkaline media [32, 33]. The current densities are normalized against ECSA to reveal the intrinsic activity of the different nanorods. The branched nanorods showed comparable peak current densities (9.42 $mA·cm^{-2}$ for the forward peak current (I_f)) to the core–shell Au@Pd nanorods (8.05 $mA·cm^{-2}$), and both are much higher than the value for the dumbbell-like nanorods (2.40 $mA·cm^{-2}$).

In spite of this, the forward peak current density of the dumbbell-like nanorods is still twice that of a commercial Pd/C catalyst (1.19 mA·cm^{-2}) with a similar Pd content. The enhanced performance could be explained by the interaction between Pd and Ag/Au, which has been reported for many bimetallic nanoparticles [34–36]. Meanwhile, the dumbbell-like nanorods show a much higher ratio of the peak current on the forward scan to that on the backward scan (i.e., I_f/I_b = 2.00), than the branched nanorods (0.89) and the core–shell Au@Pd nanorods (0.75). This result indicates a superior anti-poisoning performance of the dumbbell-like nanorods [32].

4 Conclusion

PdAg alloys have been controllably grown at different locations on gold nanorods, producing high-quality dumbbell-like and branched nanorods. The syntheses were carried out in aqueous solution at nearly room temperature, without the use of toxic or expensive reagents. Experiments suggested that the formation of PdAg alloys could be attributed to the Pd-catalyzed reduction of silver on the gold nanorods. Thus, less H_2PdCl_4 and more CTAB reduced the reaction rate for PdAg alloy formation and inhibited their nucleation on the side facets of the gold nanorods, favoring the formation of dumbbell-like nanorods. In contrast, more H_2PdCl_4 and less CTAB increased the reaction rate for PdAg formation and promoted the exposure of side facets, facilitating the formation of branched nanorods. The size and composition of PdAg alloys could be further tuned by varying the concentrations of H_2PdCl_4 and $AgNO_3$. The electrocatalytic performances of the dumbbell-like and branched PdAg–Au nanorods were examined using ethanol oxidation as a probe reaction. It was found that the branched nanorods exhibited a higher electrochemical activity, but a worse anti-poisoning performance than the dumbbell-like ones. These results concerning the preferential growth of bimetallic alloys on another metallic nanorod not only provide useful guidelines for the future control of hybrid nanostructures, but also offer potential candidates for many applications, such as heterogeneous catalysis, ultrasensitive detection and biological imaging.

Acknowledgements

This work was supported by the Natural Science Foundation of China (Nos. 20801019, 21071055, 21172076), New Century Excellent Talents in University (No. NCET-10-0369), Shandong Provincial Natural Science Foundation for Distinguished Young Scholar (No. JQ201205), Independent Innovation Foundations of Shandong University (No. 2012 ZD007), new-faculty start-up funding in Shandong University and Key Laboratory of Fuel Cell Technology of Guangdong Province.

Electronic Supplementary Material: TEM images of the as-prepared gold nanorods, EDS spectrum of the PdAg-tipped gold nanorods, the lengths and diameters of the gold nanorods and the products obtained without $AgNO_3$ or $PdCl_2$, the ECSA of the different nanorods based on the reduction of PdO_x. This material is available free of charge via the internet at http://dx.doi.org/10.1007/s12274-013-0332-8.

References

[1] Lim, B.; Jiang, M.; Camargo, P. H. C.; Cho, E. C.; Tao, J.; Lu, X.; Zhu, Y.; Xia, Y. N. Pd–Pt bimetallic nanodendrites with high actvity for oxygen reduction. *Science* **2009**, *324*, 1302–1306.

[2] Lou, L.; Yu, K.; Zhang, Z. L.; Huang, R.; Zhu, J. Z.; Wang, Y. T.; Zhu, Z. Q. Dual-mode protein detection based on Fe_3O_4-Au hybrid nanoparticles. *Nano Res.* **2012**, *5*, 272–282.

[3] Jiang, J.; Li, Y. Y.; Liu, J. P.; Huang, X. T.; Yuan, C. Z.; Lou, X. W. Recent advances in metal oxide-based electrode architecture design for electrochemical energy storage. *Adv. Mater.* **2012**, *24*, 5166–5180.

[4] Luo, Y. S.; Luo, J. S.; Jiang, J.; Zhou, W. W.; Yang, H. P.; Qi, X. Y.; Zhuang, H.; Fan, H. J.; Yu, Y. W.; Li, C. M. et al. Seed-assisted synthesis of highly ordered TiO_2@α-Fe_2O_3 core/shell arrays on carbon textiles for lithium-ion battery applications. *Energy Environ. Sci.* **2012**, *5*, 6559–6566.

[5] DeSantis, C. J.; Sue, A. C.; Bower, M. M.; Skrabalak, S. E. Seed-mediated co-reduction: A versatile route to architecturally

controlled bimetallic nanostructures. *ACS Nano* **2012**, *6*, 2617–2628.

[6] Wetz, F.; Soulantica, K.; Falqui, A.; Respaud, M.; Snoeck, E.; Chaudret, B. Hybrid Co–Au nanorods: Controlling Au nucleation and location. *Angew. Chem. Int. Ed.* **2007**, *46*, 7079–7081.

[7] Seo, D.; Yoo, C. II; Jung, J.; Song, H. Ag–Au–Ag hetero-metallic nanorods formed through directed anisotropic growth. *J. Am. Chem. Soc.* **2008**, *130*, 2940–2941.

[8] Park, K.; Vaia, R. A. Synthesis of complex Au/Ag nanorods by controlled overgrowth. *Adv. Mater.* **2008**, *20*, 3882–3886.

[9] Grzelczak, M.; Perez-Juste, J.; Garcia de Abajo, F. J.; Liz-Marzan, L. M. Optical properties of platinum-coated gold nanorods. *J. Phys. Chem. C* **2007**, *111*, 6183–6188.

[10] Camargo, P. H. C.; Xiong, Y. J.; Ji, L.; Zuo, J. M.; Xia, Y. N. Facile synthesis of tadpole-like nanostructures consisting of Au heads and Pd tails. *J. Am. Chem. Soc.* **2007**, *129*, 15452–15453.

[11] Wu, J. J.; Hou, Y. L.; Gao, S. Controlled synthesis and multifunctional properties of FePt–Au heterostructures. *Nano Res.* **2011**, *4*, 836–848.

[12] Guo, X.; Zhang, Q.; Sun, Y. H.; Zhao, Q.; Yang, J. Lateral etching of core–shell Au@metal nanorods to metal- tipped Au nanorods with improved catalytic activity. *ACS Nano* **2012**, *6*, 1165–1175.

[13] Peng, Z.; Yang, H. Synthesis and oxygen reduction electro-catalytic property of Pt-on-Pd bimetallic hetero-nanostructures. *J. Am. Chem. Soc.* **2009**, *131*, 7542–7543.

[14] Zhang, K.; Hu, X.; Liu, J.; Yin, J.; Hou, S.; Wen, T.; He, W.; Ji, Y.; Guo, Y.; Wang, Q. et al. Formation of PdPt alloy nanodots on gold nanorods: Tuning oxidase-like activities via composition. *Langmuir* **2011**, *27*, 2796–2803.

[15] Lim, B.; Jiang, M. J.; Yu, T.; Camargo, P. H. C.; Xia, Y. N. Nucleation and growth mechanisms for Pd–Pt bimetallic nanodendrites and their electrocatalytic properties. *Nano Res.* **2010**, *3*, 69–80.

[16] Wang, D. S.; Li, Y. D. Bimetallic nanocrystals: Liquid-phase synthesis and catalytic applications. *Adv. Mater.* **2011**, *23,* 1044–1060.

[17] Cortie, M. B.; McDonagh, A. M. Synthesis and optical properties of hybrid and alloy plasmonic nanoparticles. *Chem. Rev.* **2011**, *111*, 3713–3735.

[18] Wang, D. S.; Peng, Q.; Li, Y. D. Nanocrystalline intermetallics and alloys. *Nano Res.* **2010**, *3*, 574–580.

[19] Nikoobakht, B.; El-Sayed, M. A. Preparation and growth mechanism of gold nanorods using seed-mediated growth method. *Chem. Mater.* **2003**, *15*, 1957–1962.

[20] Sau, T. K.; Murphy, C. J. Seeded high yield synthesis of short Au nanorods in aqueous solution. *Langmuir* **2004**, *20*, 6414–6420.

[21] Dean, J. A. Electrolytes, Electromotive Force and Chemical Equilibrium. In *Lange's Handbook of Chemistry*, 15th Ed. McGraw-Hill Professional: New York, 1999.

[22] Wagner, C. D.; Muilenberg, G. E. Standard ESCA Spectra of the Elements and Line Energy Information. In *Handbook of X-ray Photoelectron Spectroscopy*. Perking-Elmer Corporation: MN, 1979; pp 110, 112, 154.

[23] Venezia, A. M.; Liotta, L. F.; Deganello, G.; Schay, Z.; Horvath, D.; Guczi, L. Catalytic CO oxidation over pumice supported Pd–Ag catalysts. *Appl. Catal. A* **2001**, *211*, 167–174.

[24] Ma, Y.; Bansmann, J.; Diemant, T.; Behm, R. J. Formation, stability and CO adsorption properties of PdAg/Pd(111) surface alloys. *Surf. Sci.* **2009**, *603*, 1046–1054.

[25] Liu, M. Z.; Guyot-Sionnest, P. Synthesis and optical characterization of Au/Ag core/shell nanorods. *J. Phys. Chem. B* **2004**, *108*, 5882–5888.

[26] Link, S.; Mohamed, M. B.; El-Sayed, M. A. Simulation of the optical absorption spectra of gold nanorods as a function of their aspect ratio and the effect of the medium dielectric constant. *J. Phys. Chem. B* **1999**, *103*, 3073–3077.

[27] Qiu, R.; Zhang, X. L.; Qiao, R.; Li, Y.; Kim, Y. II; Kang, Y. S. CuNi dendritic material: Synthesis, mechanism discussion, and application as glucose sensor. *Chem. Mater.* **2007**, *19*, 4174–4180.

[28] Yao, T. T.; Zhao, Q.; Qiao, Z. P.; Peng, F.; Wang, H. J.; Yu, H.; Chi, C.; Yang, J. Chemical synthesis, structural characterization, optical properties, and photocatalytic activity of ultrathin ZnSe nanorods. *Chem. Eur. J.* **2011**, *17*, 8663–8670.

[29] He, W. W.; Wu, X. C.; Liu, J. B.; Zhang, K.; Chu, W. G.; Feng, L. L.; Hu, X. N.; Zhou, W. Y.; Xie, S. S. Formation of AgPt alloy nanoislands via chemical etching with tunable optical and catalytic properties. *Langmuir* **2010**, *26,* 4443–4448.

[30] He, W. W.; Wu, X. C.; Liu, J. B.; Zhang, K.; Chu, W. G.; Feng, L. L.; Hu, X. N.; Zhou, W. Y.; Xie, S. S. Pt-guide formation of Pt–Ag nanoislands on Au nanorods and improved methanol electro-oxidation. *J. Phys. Chem. C* **2009**, *113*, 10505–10510.

[31] Xiang, Y. J.; Wu, X. C.; Liu, D. F.; Jiang, X. Y.; Chu, W. G.; Li, Z. Y.; Ma, Y.; Zhou, W. Y.; Xie, S. S. Formation of rectangularly shaped Pd/Au bimetallic nanorods: Evidence for competing growth of the Pd shell between the {110} and {100} side facets of Au nanorods. *Nano Lett.* **2006**, *6*, 2290–2294.

[32] Du, W.; Mackenzie, K. E.; Milano, D. F.; Deskins, N. A.; Su, D.; Teng, X. Palladium–Tin alloyed catalysts for the

ethanol oxidation reaction in an alkaline medium. *ACS Catal.* **2012**, *2*, 287–297.

[33] Zhang, G. R.; Wu, J.; Xu, B. Q. Syntheses of Sub-30 nm Au@Pd concave nanocubes and Pt-on-(Au@Pd) trimetallic nanostructures as highly efficient catalysts for ethanol oxidation. *J. Phys. Chem. C* **2012**, *116*, 20839–20847.

[34] Cui, C. H.; Yu, J. W.; Li, H. H.; Gao, M. R.; Liang, H. W.; Yu, S. H. Remarkable enhancement of electrocatalytic activity by tuning the interface of Pd–Au bimetllic nanoparticle tubes. *ACS Nano* **2011**, *5*, 4211–4218.

[35] Kang, S. W.; Lee, Y. W.; Kim, M.; Hong, J. W.; Han, S. W. One-pot synthesis of carbon-supported dendritic Pd–Au nanoalloys for electrocatalytic ethanol oxidation. *Chem. Asian J.* **2011**, *6*, 909–913.

[36] Li, G. L.; Jiang, L. H.; Jiang, Q.; Wang, S. L.; Sun, G. Q. Preparation and characterization of Pd_xAg_y/C electrocatalysts for ethanol electrooxidation reaction in alkaline media. *Electrochim. Acta* **2011**, *56*, 7703–7711.